The American Journal of Pathology, Vol. 192, No. 8, August 2022

ELSEVIER

The American Journal of PATHOLOGY

ajp.amjpathol.org

CELL INJURY, REPAIR, AGING, AND APOPTOSIS

Neonatal Enthesis Healing Involves Noninflammatory Acellular Scar Formation through Extracellular Matrix Secretion by Resident Cells

Ron C. Vinestock,* Neta Felsenthal,* Eran Assaraf,* Eldad Katz,* Sarah Rubin,* Lia Heinemann-Yerushalmi,* Sharon Krief,* Nili Dezorella,† Smadar Levin-Zaidman,† Michael Tsoory,‡ Stavros Thomopoulos,§¶ and Elazar Zelzer*

From the Departments of Molecular Genetics, Electron Microscopy Unit,† and Veterinary Resources,‡ Weizmann Institute of Science, Rehovot, Israel; and the Departments of Orthopedic Surgery§ and Biomedical Engineering,¶ Columbia University, New York, New York*

Accepted for publication May 4, 2022.

Address correspondence to Elazar Zelzer, Ph.D., Arthur and Rochelle Belfer Building for Biomedical Research, Weizmann Institute of Science, Rehovot 7610001, Israel. E-mail: eli.zelzer@weizmann.ac.il.

Wound healing typically recruits the immune and vascular systems to restore tissue structure and function. However, injuries to the enthesis, a hypocellular and avascular tissue, often result in fibrotic scar formation and loss of mechanical properties, severely affecting musculoskeletal function and life quality. This raises questions about the healing capabilities of the enthesis. Herein, this study established an injury model to the Achilles entheses of neonatal mice to study the effectiveness of early-age enthesis healing. Histology and immunohistochemistry analyses revealed an atypical process that did not involve inflammation or angiogenesis. Instead, healing was mediated by secretion of collagen types I and II by resident cells, which formed a permanent hypocellular and avascular scar. Transmission electron microscopy showed that the cellular response to injury, including endoplasmic reticulum stress, autophagy, and cell death, varied between the tendon and cartilage ends of the enthesis. Single-molecule *in situ* hybridization, immunostaining, and terminal deoxynucleotidyl transferase-mediated dUTP nick-end labeling assays verified these differences. Finally, gait analysis showed that these processes effectively restored function of the injured leg. These findings reveal a novel healing mechanism in neonatal entheses, whereby local extracellular matrix secretion by resident cells forms an acellular extracellular matrix deposit without inflammation, allowing gait restoration. These insights into the healing mechanism of a complex transitional tissue may lead to new therapeutic strategies for adult enthesis injuries. *(Am J Pathol 2022, 192: 1122–1135; https://doi.org/10.1016/j.ajpath.2022.05.008)*

Wound healing is a critical and complex process that restores structure and function by replacing damaged tissue. In adult animals, this process comprises a sequential cascade of overlapping events, including bleeding and activation of the coagulation system, recruitment of inflammatory cells, fibroblast migration, collagen synthesis, angiogenesis, and remodeling of the injury site.[1,2] In the musculoskeletal system, however, tissues differ in their ability to heal injuries.[3] Although bones and muscles have regenerative capacities,[4,5] tendon, ligament, and cartilage tissues often heal via scar formation, without complete restoration of mechanical properties. Interestingly, these scar-forming tissues are all extracellular matrix (ECM) rich, hypocellular, poorly vascularized, and slow proliferating, all of which may influence the repair process.[6–8]

Tendon, ligament, and cartilage healing have been investigated using a variety of injury models in different organisms.[6,9] In tendons, common injury models include full or partial transection of the tendon and overuse injuries

Supported by NIH grant R01AR055580 (S.T. and E.Z.), Israel Science Foundation grant 1462/20, Minerva Foundation grant 713533, the David and Fela Shapell Family Center for Genetic Disorders, and the Estate of Mr. and Mrs. van Adelsbergen (E.Z.). M.T. is the incumbent of the Carolito Stiftung Research Fellow Chair in Neurodegenerative Diseases.

R.C.V. and N.F. contributed equally to this work.

Disclosures: None declared.

https://doi.org/10.1016/j.ajpath.2022.05.008

caused by physical activities.[10–12] During the healing process, recruited fibroblasts initially synthesize predominantly collagen type III (COL3A1), later replacing it with collagen type I (COL1A1). However, this remodeling process is typically insufficient, often resulting in an altered ECM composition compared with the uninjured tissue.[13] Thus, the repair of injured adult tendons usually involves formation of a fibrovascular scar and loss of histologic and mechanical characteristics.[13,14] However, a recent study in neonatal mice showed regenerative properties of Achilles tendon after transection.[10]

Studies of cartilage repair have established different healing responses in partial-thickness compared with full-thickness injuries. Partial-thickness injuries do not heal spontaneously, as inflammation and blood vessels are absent.[15] Following injury, cells within the wound margins undergo chondroptosis, a variant of cell death that is characterized by an increase in Golgi apparatus and endoplasmic reticulum (ER), autophagic vacuoles, patchy condensations of nuclei, blebbing of cytoplasmic material, and activation of apoptosis via caspase-3 and caspase-9 involvement.[16–21] In full-thickness injuries, the damage is deeper and reaches into the subchondral bone, thereby generating a pathway into the vascularized bone marrow. This enables access for the recruitment of immune cells, eventually leading to fibrocartilage formation and ECM deposition in the wound area. As the newly formed fibrocartilage is weaker than the original tissue, the cartilage undergoes gradual degradation, which leads to loss of mechanical properties.[22–24]

Another component of the musculoskeletal system is the enthesis, a fibrocartilaginous tissue that bridges tendon and bone. This unique specialized connective tissue attaches the two distinct tissues by forming a gradient of cellular and extracellular features along its length.[25,26] Adult enthesis repair commonly results in permanent damage because of failure to restore its structure. The resulting mechanically insufficient attachment limits joint function and is prone to retears.[27] However, the outcome may depend on the severity and type of injury. Comparison of the mechanical outcomes of rotator cuff injuries in adult mice suggest that repair is more successful after partial injuries, including reduced scar formation and recovery of gait.[28] Furthermore, rotator cuff entheses of neonatal mice display some regenerative capacity.[29]

The difference in healing potential between adult and neonatal mice raises the possibility that the healing capacity of the enthesis is switched off early after birth. Moreover, given the complexity of the enthesis structure, it is unclear whether the healing process, if exists, follows the same course in all enthesis zones. To address these questions, needle-punch injury was induced to neonatal Achilles enthesis, an injury model that minimizes damage to surrounding tissues or penetration into the bone marrow space. Although no inflammation or angiogenesis was observed, temporal analyses identified the formation of an acellular domain and ECM plug at the injury site. The acellular domain was composed of COL1A1 at the tendon end and collagen type II (COL2A1) at the cartilage end, suggesting that this domain is formed locally by the resident enthesis cells. Immunostaining, gene expression analyses, terminal deoxynucleotidyl transferase-mediated dUTP nick-end labeling (TUNEL) assay, and transmission electron microscopy (TEM) revealed that cells at the injury site undergo ER stress and autophagy, and suggested that the observed cellular loss was a result of chondroptosis-like cell death. Gait recovery suggested that, despite the loss of tissue structure, the healing process effectively restored joint function. Together, these findings reveal a novel mechanism in neonatal mice whereby extensive secretion of ECM by resident cells at the injury site drives enthesis healing and restores its function.

Materials and Methods

Mice

All experiments involving mice were approved by the Institutional Animal Care and Use Committee of the Weizmann Institute of Science (Rehovot, Israel). Histology was performed on C57BL6 wild-type mice. Green fluorescent protein (GFP)—LC3#53 mice were kindly provided by Prof. Zvulun Elazar (Weizmann Institute of Science).

Achilles Enthesis Injury Model

Postnatal day 7 neonatal mice were anesthetized by lidocaine (0.03 mg, intraperitoneally). A small incision was made through the skin to expose the Achilles enthesis and was needle punched using a 32-gauge needle using a sterile approach. The skin was then sutured with nylon 5/0 monofilament. The left limb was used as a control. After injury, the animals returned to full cage activity. Sex distribution was equal.

Histologic Analysis, TUNEL, and Von Kossa Staining

For histology, postnatal mice were harvested at various ages, dissected, and fixed in 4% paraformaldehyde (PFA)/phosphate-buffered saline (PBS) at 4°C overnight. After fixation, tissues were dehydrated to 70% ethanol and embedded in paraffin. Pup and adult tissues were decalcified using 0.5 mol/L EDTA (pH 7.4) before dehydration. The embedded tissues were cut to generate sections (7 μm thick) and mounted onto slides.

Hematoxylin and eosin and Safranin O stains were performed following standard protocols. TUNEL assay was performed using *In Situ* Cell Death Detection Kit (Roche, Mannheim, Germany), according to the manufacturer's protocol.

For Von Kossa and toluidine blue (pH 6.0) staining, fixed calcified tissues were embedded in optimal cutting temperature compound. Cryosections (10 μm thick) were prepared using the Kawamoto film method,[30] and staining was performed using standard protocols.[31] In short, postnatal mice were harvested at 5 months after injury, dissected, and fixed

in 4% PFA/PBS at 4°C overnight. After fixation, tissues were transferred to 30% sucrose overnight, then embedded in OCT and sectioned by cryostat at a thickness of 10 μm. Slides were incubated in 1% silver nitrate solution for 2.5 minutes in UV table, then rinsed three times in distilled water. Unreacted silver was removed by 5-minute incubation in 5% sodium thiosulfate, then rinsed in water. Then, sections were counterstained with toluidine blue. Last, slides were mounted with Entellan (Sigma-Aldrich, St. Louis, MO; 1079600500).

Immunofluorescence

For immunohistochemistry on paraffin sections, animals were harvested at various ages, dissected, and fixed in 4% PFA/PBS at 4°C overnight. After fixation, tissues were decalcified using 0.5 mol/L EDTA (pH 7.4), washed thoroughly with water, dehydrated to 70% ethanol, and embedded in paraffin. The embedded tissues were cut to generate sections (7 μm thick) and mounted onto slides. Antigen retrieval for anti-collagen types I, II, and III antibodies was performed using 1.8 μg proteinase K (P9290; Sigma-Aldrich) in 200 mL PBS for 10 minutes. Antigen retrieval for anti-GFP, F4/80, and cleaved caspase-3 antibodies was performed in 10 mmol/L sodium citrate buffer (pH 6.0) cooked in 80°C for 15 minutes in a hot tub. Then, sections were washed twice in PBS, and endogenous peroxidase was quenched using 3% H_2O_2 in PBS. Non-specific binding was blocked using 7% horse serum and 1% bovine serum albumin dissolved in PBS−Tween 20 (PBST) for 1 hour. Then, sections were incubated with rabbit anti-collagen I antibody (1:100; number NB600-408; Novus Biologicals, Littleton, CO), mouse anti-collagen II antibody (1:50; II-II6B3; Developmental Studies Hybridoma Bank, Iowa City, IA), rabbit anti-collagen III (1:100; ab7778; Abcam, Cambridge, UK), goat anti-GFP (biotin) antibody (1:100; ab6658; Abcam), rabbit anti-cleaved caspase-3 (Asp175) antibody (1:200; number 9664s; Cell Signaling Technology, Danvers, MA), or rat anti-F4/80 antibody (1:50; ab6640; Abcam) overnight at room temperature. The next day, sections were washed twice in PBST and incubated with biotin anti-rabbit (1:100; Jackson ImmunoResearch, West Grove, PA), or biotin anti-rat (1:100; Jackson ImmunoResearch), for 1 hour at room temperature. Then, after two washes of PBST, slides were incubated with streptavidin-Cy2 or streptavidin-Cy3 (1:100; Jackson ImmunoResearch) and Cy3-conjugated donkey anti-mouse (1:100; Jackson ImmunoResearch). Occasionally, slides were counterstained using DAPI. Then, slides were mounted with Shandon Immu-mount (number 9990402; Thermo Fisher Scientific, Waltham, MA).

For immunohistochemistry on cryosections, animals were harvested at various ages, dissected, and fixed in 4% PFA/PBS at 4°C overnight. Then, tissues were decalcified using 0.5 mol/L EDTA (pH 7.4) and transferred to 30% sucrose overnight, embedded in OCT, and sectioned by cryostat at a thickness of 10 μm. Cryosections were dried and post-fixed for 20 minutes in acetone at −20°C. Then, sections were permeabilized with 0.2% Triton/PBS. To block non-specific binding of Ig, sections were incubated with 7% goat serum in PBS. Cryosections were then incubated overnight at 4°C with primary antibody rat anti-mouse CD31 (PMG550274; 1:50; BD Pharmingen, San Diego, CA). The next day, sections were washed in PBS and incubated with biotin anti-rabbit (1:100; Jackson ImmunoResearch). Then, slides were incubated with streptavidin-Cy3 (1:100; Jackson ImmunoResearch) and Cy3-conjugated donkey anti-rabbit (1:100; Jackson ImmunoResearch). Occasionally, slides were counterstained using DAPI. Then, slides were mounted with Shandon Immu-mount.

Transmission Electron Microscopy

Animals were harvested at 1 and 3 days and 5 months after injury, dissected, and fixed with 3% paraformaldehyde and 2% glutaraldehyde in 0.1 mol/L cacodylate buffer containing 5 mmol/L $CaCl_2$ (pH 7.4) overnight. The tissue was decalcified using 0.5 mol/L EDTA (pH 7.4) for 96 hours. Vibrotome sections (200 μm thick) were prepared (VT1000 S; Leica, Wetzlar, Germany), and tissue was postfixed in 1% osmium tetroxide supplemented with 0.5% potassium hexacyanoferrate trihydrate and potassium dichromate in 0.1 mol/L cacodylate (1 hour), stained with 2% uranyl acetate in water (1 hour), dehydrated in graded ethanol solutions, and embedded in Agar 100 epoxy resin (Agar Scientific Ltd, Stansted, UK). Ultrathin sections (70 to 90 nm thick) were obtained with a Leica EMUC7 ultramicrotome and transferred to 200-mesh copper TEM grids (SPI, West Chester, PA). Grids were stained with lead citrate and examined with an FEI Tecnai SPIRIT (FEI, Eidhoven, the Netherlands) TEM operated at 120 kV and equipped with a OneView camera (Gatan, Pleasanton, CA).

Single-Molecule Fluorescent *in Situ* Hybridization

Single-molecule fluorescence *in situ* hybridization was performed using hybridization chain reaction (HCR) version 3.0, as previously described[32] with slight modifications. The probes for *BiP* and *CHOP* were both designed and ordered from Molecular Instruments (Los Angeles, CA). mRNA accession numbers are shown in Table 1. Briefly, tissue was fixed for 3 hours following sacrifice using 4% PFA/PBS freshly prepared with diethyl pyrocarbonate water. Then, solution was changed to 4% PFA/PBS/30% sucrose and was incubated by shaking overnight. The following day, the tissue was embedded in OCT and kept at −80°C until use. On the morning of the experiment, the tissue blocks were cut to produce sections (10 μm thick) using a cryostat, and kept in the cryostat chamber at −30°C until the beginning of the experiment. Then, tissue sections were warmed to room temperature and dried in a chemical hood for 7 minutes, followed by incubation in 70% ethanol/diethyl pyrocarbonate at 4°C for 1 hour. Then, sections were washed once in PBS and fixed in 4% RNase-free PFA for 7 minutes, washed with RNAse-free PBS, and permeabilized in 10 μg/mL proteinase K/PBS for 10 minutes at room

Table 1 List of Probes Used for *in Situ* Hybridization Chain Reaction and Their Accession Numbers

Probe name	Accession no.	HCR amplifier	Amplifier color, nm
BiP	NM_022310.3	B5	546
CHOP	NM_007837.4	B3	488

Accession numbers from *https://www.ncbi.nlm.nih.gov/nuccore* (last accessed June 7, 2022).

temperature. Sections were then washed with RNAse-free PBS−Tween 0.1% twice, post-fixed with 4% RNase-free PFA for 5 minutes, and washed again with RNAse-free PBS−Tween 0.1% twice for 5 minutes. Then, sections were washed with acetylation buffer for 10 minutes, washed twice with RNAse-free PBS−Tween 0.1%, and rinsed in diethyl pyrocarbonate, as previously described by Shwartz and Zelzer.[33] Next, sections were left to dry for 30 minutes at room temperature and equilibrated in HCR hybridization buffer (Molecular Instruments) for 10 minutes at 37°C. Probes were then added to the sections at a final concentration of 0.4 to 4 nmol/L and hybridized overnight in a humidified chamber at 37°C. The next day, the protocol described by Choi et al[32] was applied using home-made wash buffer [50% formamide (75-12-7; Merck Millipore, Darmstadt, Germany), 5× saline-sodium citrate (Molecular Biology-P; 001985232300; Bio-Lab Ltd., Jerusalem, Israel), 9 mmol/L citric acid (pH 6.0; 77-92-9; Sigma Aldrich, Darmstadt, Germany), 0.1% Tween 20 (P1279; Sigma Aldrich), and 50 μg/mL heparin (H3393; Sigma Aldrich)]. The probe sets were amplified with HCR hairpins for 45 minutes at room temperature in HCR amplification buffer (Molecular Instruments). Fluorescently conjugated DNA hairpins used in the amplification were ordered from Molecular Instruments. Before use, the hairpins were snap cooled by heating at 95°C for 90 seconds and cooling to room temperature for 30 minutes in the dark. After amplification, the samples were washed in 5× saline-sodium citrate−Tween 20 and stained with DAPI (1:10,000; D9542; Millipore Sigma, Rehovot, Israel) diluted in PBS for 5 minutes and then mounted onto slides using Shandon Immu-mount.

Sections were imaged with a confocal LSM 800 microscope (Zeiss, Jena, Germany) at a resolution of 70 nm (x, y). The brightness of the *in situ* signal was enhanced in FIJI version 1.53c (*https://fiji.sc*) for presentation in the figure.[34] For quantification of transcripts per cell, amplification was performed for 1 hour, and sections were imaged with the same microscope at a resolution of 70 and 400 nm (x, y, z). Autofluorescence imaging of cells was acquired with excitation at 488-nm laser, and cells were segmented with cellpose (green), using the cyto algorithm with a diameter size between 75 and 500 pixels, depending on the area in the enthesis. Images were then further quantified in CellProfiler version 3.1.9 (*https://cellprofiler.org*) with custom pipelines.[35] Five sections of each zone (tendon end, mid-enthesis, and cartilage end) of three animals were measured; in total, there were 2228 cells of injured limbs and 2413 cells of control limbs.

Quantitative Real-Time PCR

Achilles entheses were removed from 1-day postinjury mice using a surgical blade. At this age, the cartilaginous end marking the enthesis is distinguishable from the rest of the calcaneus by its bright white color. Measuring approximately 0.5 mm, the white extremity along with the attached tendon was isolated and homogenized. Total RNA was purified using the RNeasy Kit (Qiagen, Hilden, Germany). Reversed transcription was performed with High-Capacity cDNA Reverse Transcription Kit (Applied Biosystems, Waltham, MA), according to the manufacturer's protocol. Quantitative real-time PCR was performed using Fast SYBR Green master mix (Applied Biosystems) on the StepOnePlus machine (Applied Biosystems). Values were calculated using the StepOne software version 2.2, according to the relative standard curve method. For each gene, fold change relative to the control was calculated by delta-delta cycle threshold method. Data were normalized to *18S* rRNA. Primer sequences are given in Table 2.

Functional Recovery Assessment: CatWalk Gait Analysis

Gait and stride were assessed using the CatWalk XT 10.6 automated gait analysis system (Noldus Information Technology, Wageningen, the Netherlands) at 14, 28, and 56 days after manipulation (enthesis injury or sham operation). Mice were subjected to at least five runs in each assessment session. Following the identification and labeling of each footprint, gait data were generated. Functionality was assessed as in previous studies of recovery from nerve or enthesis damage[28,36–38] using the following indices: maximum contact area, which is the area (cm^3) of the foot touching the surface during the time of maximum contact; print area, which is the surface area of the complete print; and stand, which is the duration in seconds of contact of a paw with the glass plate. The ratio between the contact area made by the manipulated hind limb (right) relative to that of the intact hind limb (left) was calculated and used for statistical analyses.

Table 2 List of Primers Used for the Quantitative Real-Time PCR and Their Sequences

Primer name	Forward sequence	Reverse sequence
BiP	5′-GGGGACCACCTATTCCTGCGTC-3′	5′-ATACGACGGCGTGATGCGGT-3′
CHOP	5′-TGTTGAAGATGAGCGGGTGGCA-3′	5′-GGACCAGGTTCTGCTTTCAGGTGT-3′
18S rRNA	5′-GTAACCCGTTGAACCCCATT-3′	5′-CCATCCAATCGGTAGTAGCG-3′

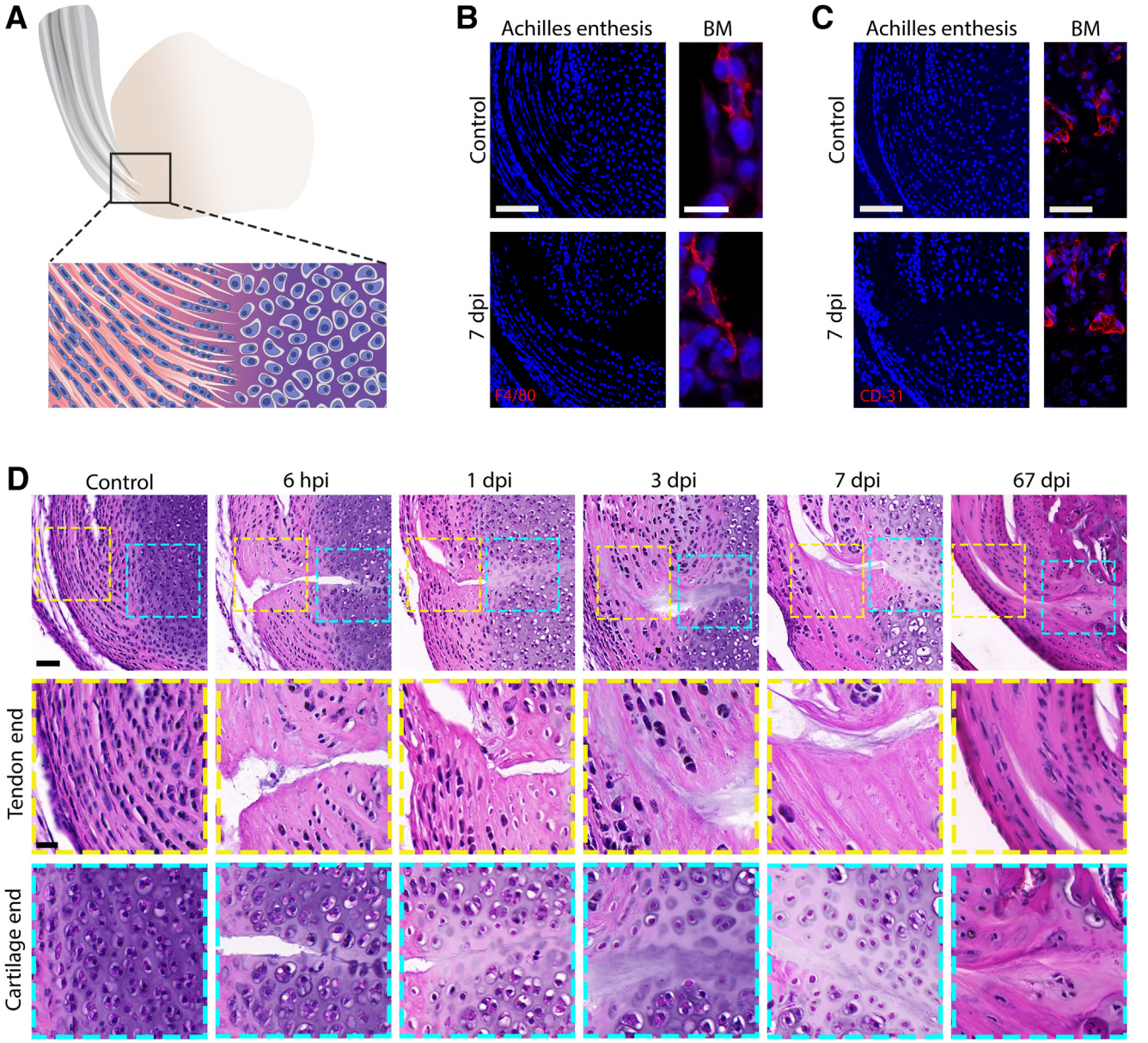

Figure 1 Enthesis healing involves formation of hypocellular domains flanking an extracellular matrix plug without typical features of wound healing. **A:** Schematic illustration of the Achilles enthesis. **B:** F4/80 immunohistochemistry staining of sections through the enthesis at 7 days after injury (dpi) shows no macrophages in proximity to the injury site. Bone marrow (BM) was used as a positive control. **C:** CD31 immunohistochemistry staining at 7 dpi shows no angiogenesis at the injury site. Bone marrow was used as a positive control. **D:** Hematoxylin and eosin staining of sagittal sections of postnatal day 7 control uninjured entheses and injured entheses at 6 hours after injury (hpi) to 67 dpi. **Yellow** and **teal boxed areas** are magnifications of the tendon end and cartilage end, respectively. $n = 3$ (**B** and **C**); $n = 4$ at 6 hpi and 7 and 67 dpi (**D**); $n = 8$ at 1 dpi (**D**); $n = 10$ at 3 dpi (**D**). Scale bars: 100 μm (**B** and **C**, 7 dpi); 10 μm (**B**, control); 50 μm (**C**, control, and **D**, **top panels**); 20 μm (**D**, **middle and bottom panels**).

Statistical Analysis

Statistical analyses of quantitative real-time PCR results were performed with Excel (Microsoft, Redmond, WA) using paired two-tailed *t*-test. CatWalk gait analyses were performed using SPSS version 23 (IBM, Armonk, NY). Two-factor analysis of variance was followed by planned comparisons (independent-sample *t*-test and one-sample *t*-test). Quantification of single-molecule fluorescence *in situ* hybridization HCR results was performed using linear mixed model. The data are presented as means ± SD. All statistical details, including *n* values, are given in the figures and figure legends.

Results

The Neonatal Enthesis Heals by Formation of Hypocellular Domains Flanking an ECM Plug

To study the healing process of the enthesis, we established a mouse model of partial injury (Figure 1A). Using postnatal

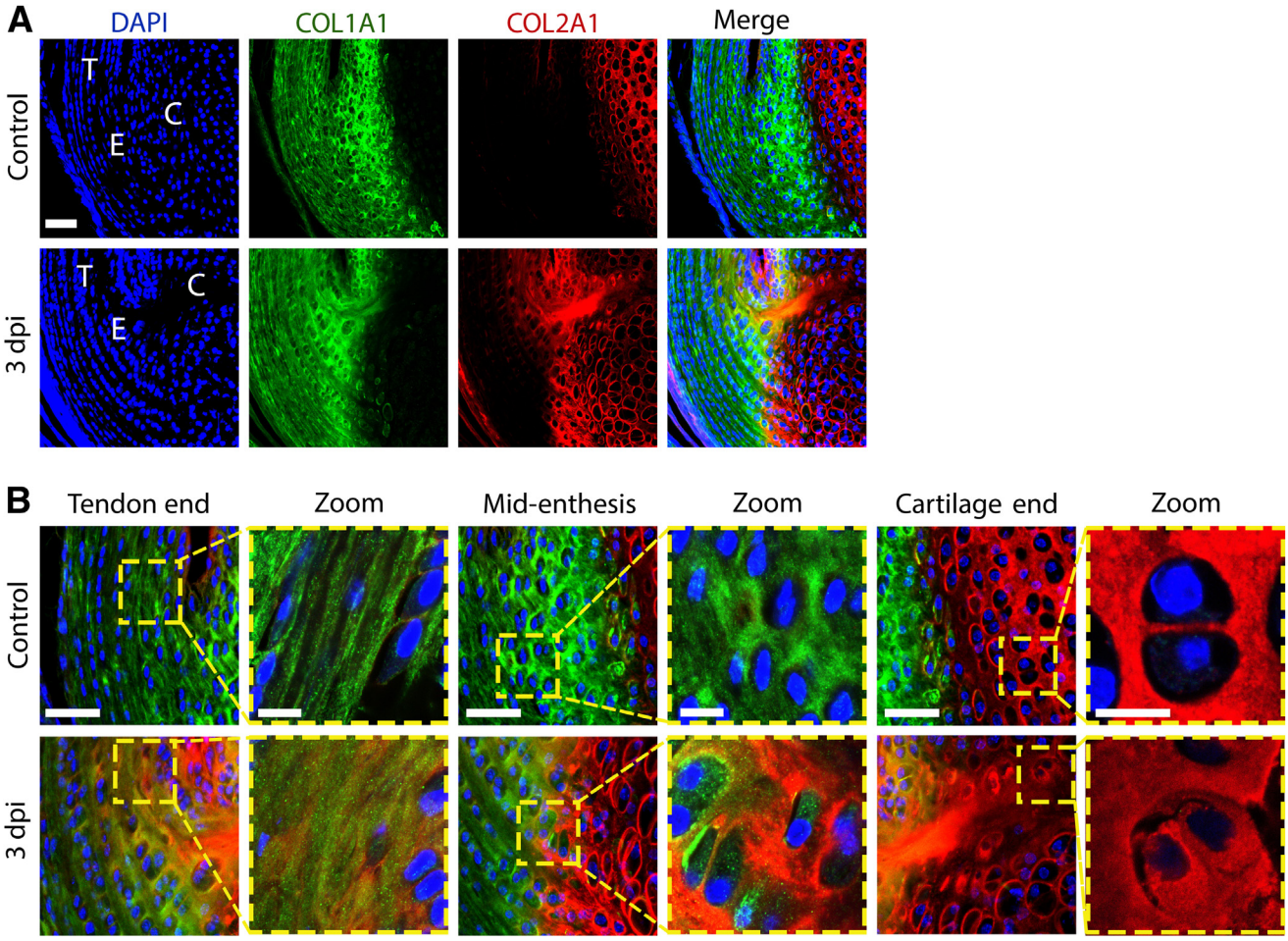

Figure 2 Enthesis cells form a local acellular scar by secreting collagen type I (COL1A1) and collagen type II (COL2A1). **A:** Immunohistochemistry staining for COL1A1 and COL2A1 shows extracellular matrix plug and loss of expression domain in 3 days after injury (dpi) enthesis (E) in comparison to the control. **B:** Magnifications of tendon (T), enthesis, and cartilage (C) in control and 3-dpi entheses. Yellow boxes are magnifications of the **boxed areas**. $n = 12$ (**A**). Scale bars: 50 μm (**A**); 20 μm (**B**, tendon end, mid-enthesis, and cartilage end images); 10 μm (**B**, zoom images).

day 7 mice, a minimal cut of the skin was performed and a thin 32-gauge needle was inserted through the tendon and the Achilles enthesis, reaching the distal part of the calcaneus. This procedure injured the enthesis throughout its length, while avoiding penetration of the bone marrow cavity and bleeding, thereby excluding the potential contribution of cells from the marrow space. Notably, as the mouse enthesis mineralizes at approximately 2 weeks postnatally, the injury was made in an unmineralized enthesis.

Following the classic model of wound healing, the injury site was examined for the presence of inflammation. For that, day 7 postinjury and noninjured limb sections were immunostained for F4/80, a specific marker for macrophages.[39] As seen in Figure 1B and Supplemental Figure S1, no macrophages were detected in or around the injury site. To determine whether there was angiogenesis in the injured enthesis, endothelial marker CD31 staining was performed[40] (Figure 1C and Supplemental Figure S2). The results showed no blood vessel invasion into the injury site. Together, these results suggested that in our enthesis injury model, healing did not involve inflammation and angiogenesis.

To uncover the temporal profile of the healing process, histologic sections were analyzed through the enthesis at 6 hours and 1, 3, 7, and 67 days after injury (dpi). As seen in Figure 1D, at 6 hours, the injury site was clearly observed as a cut that extended between the Achilles tendon across the enthesis to the distal cartilage end of the calcaneus. Interestingly, at day 3 after injury, in the region of the injury site near the tendon, an acellular domain was forming and propagating several cell rows away from the injury margins. At the yet unmineralized cartilage end of the enthesis, a similar propagation of the response area away from the injury site was observed. Chondrocytes adjacent to the injury site lost most of their volume, whereas the matrix around them appeared abnormal, as it was paler than in the control. Within the injury site, accumulation of ECM filled part of the gap, forming a plug-like structure. In line with the macrophage and endothelial cell results, there were no

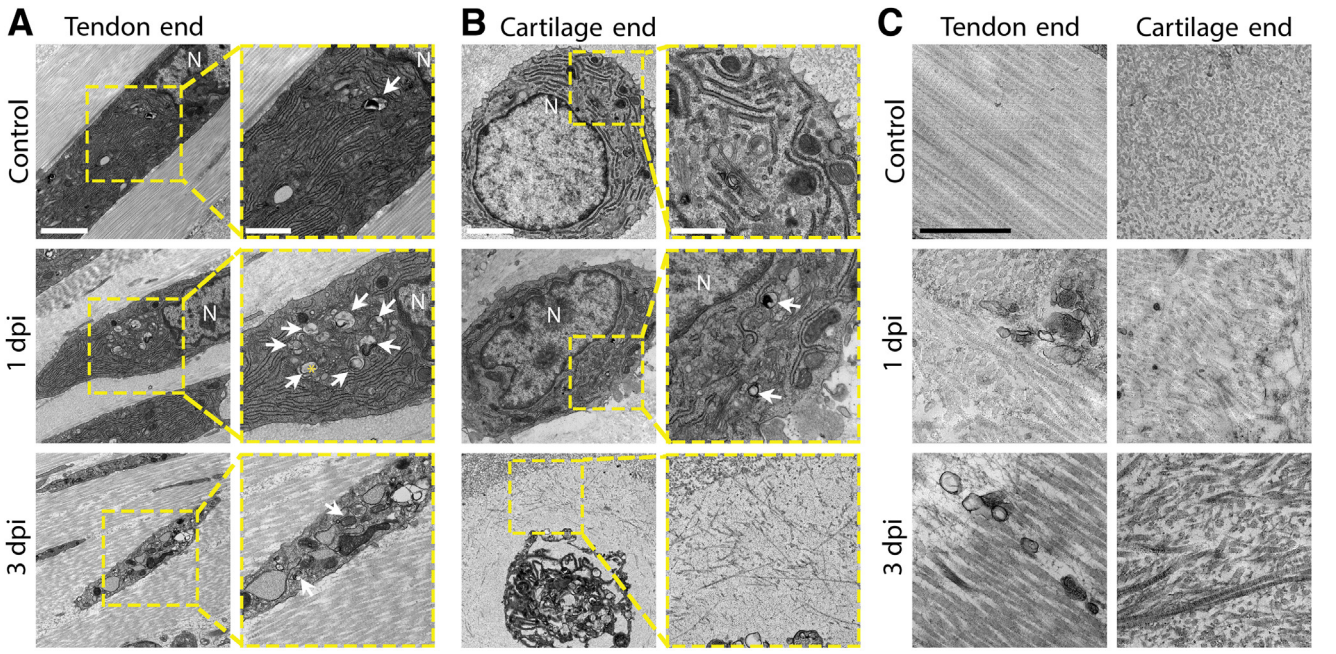

Figure 3 Transmission electron microscopy reveals impaired cellular and extracellular matrix (ECM) morphology in the healing enthesis. **A:** Cellular morphology at the tendon end of control, 1-day after injury (dpi), and 3-dpi entheses. Yellow boxes are magnifications of the **boxed areas**. **B:** Cellular morphology at the cartilage end of control, 1-dpi, and 3-dpi entheses. Yellow boxes are magnifications of the **boxed areas**. **C:** Fiber orientation of the ECM plug at the tendon end and cartilage end of control, 1-dpi, and 3-dpi entheses. **Arrows** mark autophagic vacuoles. Scale bars: 2 μm (**A**, tendon end images, and **B**, cartilage end images); 1 μm (**A** and **B**, **yellow boxes**, and **C**). N, nucleus.

signs of inflammation or angiogenesis at the injury site. At 7 dpi, the injury site was still recognizable. The area around it remained acellular, an ECM plug filled the gap, and the proximate cells at both tendon and cartilage ends of the enthesis displayed loss of cellular features. This morphology of the injury site was unchanged at 67 dpi.

To evaluate long-term remodeling of the injured enthesis, mineralization was examined by staining sections with Von Kossa stain at 5 months after injury. As seen in Supplemental Figure S3, the healed enthesis was mineralized; however, the tidemark, which typically borders between mineralized and nonmineralized parts of the fibrocartilage enthesis, was disrupted, indicating a failure of the enthesis to heal completely.

Collectively, the absence of inflammation and angiogenesis and the formation of hypocellular domains flanking an ECM plug suggested that the enthesis can heal via a novel mode of tissue repair.

Hypocellular Scar at the Healing Neonatal Enthesis Is Formed Locally by Resident Cells

Previous studies on enthesis healing described the formation of a scar tissue enriched with COL3A1.[41,42] To examine if the observed hypocellular scar in the injury site was composed of COL3A1, we immunostained 3 dpi and control limbs for COL3A1. As seen in Supplemental Figure S4, no changes in the level of COL3A1 in or around the injury site were observed.

The two main components of the enthesis ECM are COL1A1, which is expressed in the tendon and its transition into fibrocartilage; and COL2A1, which is expressed in the fibrocartilage and its transition into bone. Having observed the formation of an ECM plug in the healing enthesis, the study examined the distribution of these two collagens during the healing process. For that, double-immunofluorescence staining for COL1A1 and COL2A1 was performed on sections of 1, 3, and 7 dpi and age-matched uninjured Achilles entheses (Figure 2A and Supplemental Figures S5 and S6). In control entheses, the expected patterns of expression were seen, as COL1A1 was expressed in the tendon and the enthesis, whereas COL2A1 was expressed across cartilage, with limited overlap between the domains.

In the injured enthesis, at 1 dpi, we observed accumulation of COL1A1 and COL2A1 at the injury site (Supplemental Figure S5); and at 3 and 7 dpi, the hypocellular domain and ECM plug were positive for COL1A1 and COL2A1. Interestingly, the overall patterns of expression were maintained, suggesting that the ECM plug forms locally by the cells flanking the injury site. Nevertheless, we observed that, in the injured enthesis, COL2A1 expression expanded into the tendon end, whereas in the ECM plug, the two expression domains expanded into each other.

To gain a better understanding of the loss of segregation between COL1A1 and COL2A1 expression domains, the cells at the border between the two domains were examined at higher magnification. As seen in Figure 2B, although cells

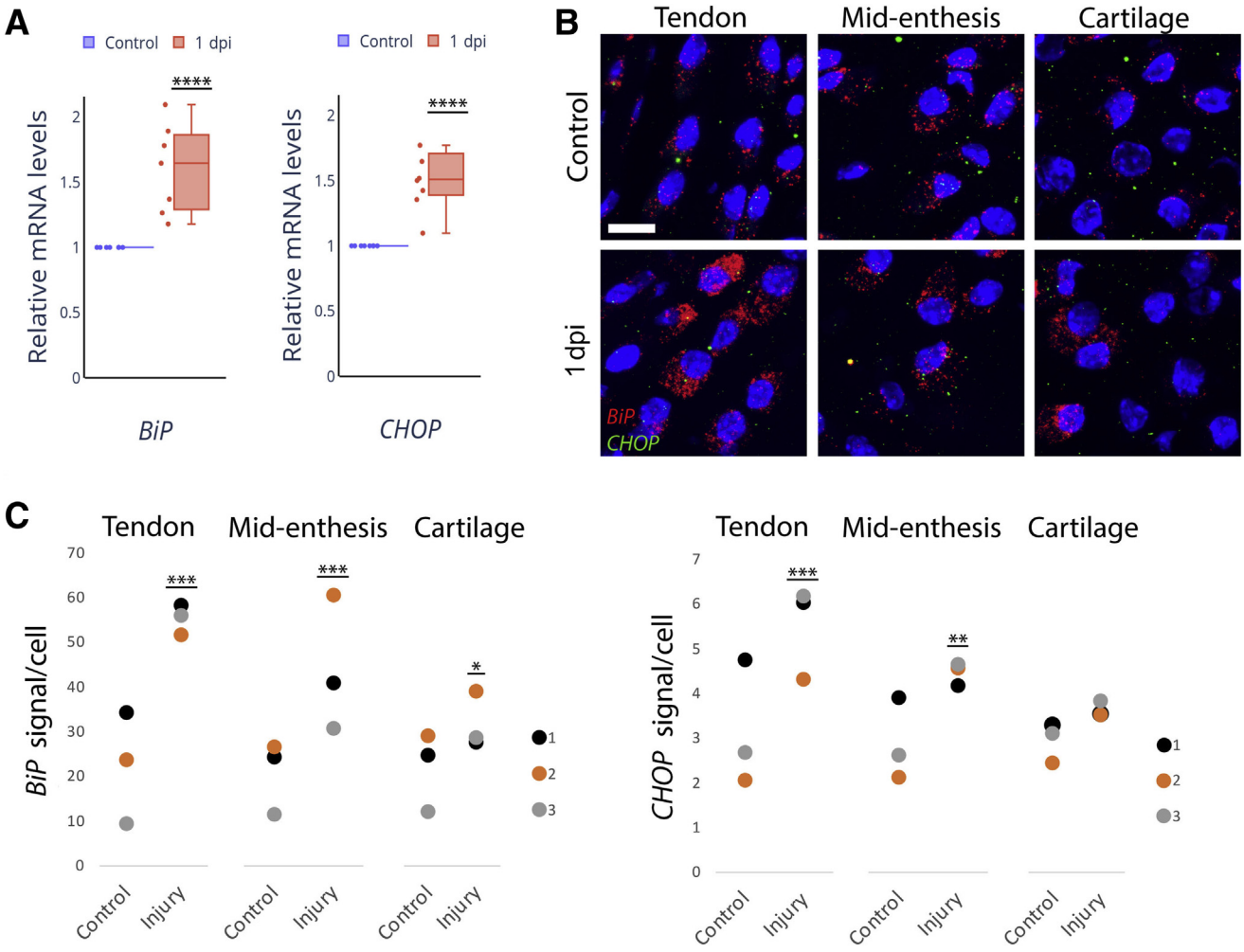

Figure 4 Up-regulation in endoplasmic reticulum (ER) stress markers in 1-day after injury (dpi) enthesis. **A:** Graph showing quantitative real-time PCR analysis for *BiP* and *CHOP* mRNA in control and 1-dpi entheses (data are normalized to *18S*). **B:** Single-molecule fluorescence *in situ* hybridization (smFISH) for ER stress markers *BiP* and *CHOP* reveals an elevation in expression levels in 1-dpi enthesis. **C:** Graph showing the ratio of quantified smFISH signal of *BiP* and *CHOP* per cell in tendon, enthesis, and cartilage regions of control and 1-dpi animals. Color coding indicates paired comparison samples. Data are presented as means ± SD (**A**) or means (**C**). $n = 7$ (**A**); $n = 3$ (**C**). $^{*}P < 0.05$, $^{**}P < 0.01$, $^{***}P < 0.001$, and $^{****}P < 0.0001$. Scale bar = 10 μm (**B**).

in the uninjured enthesis expressed only one type of collagen, same-stage cells of injured enthesis that co-expressed COL1A1 and COL2A1 were observed. In addition, although in the uninjured enthesis COL2A1 staining was observed in the ECM around the cells, at the cartilage end adjacent to the injury site, where histologically the study identified shrinking chondrocytes, the empty lacunae of these cells were mostly COL2A1-positive and DAPI-negative.

These results suggested that the hypocellular domain around the injury site is formed by ECM secretion by neighboring local cells, which divides this domain into two regions containing either tendon or cartilage ECM. At the border between them, cells co-express COL1A1 and COL2A1, resulting in mixed ECM. Although the composition of the ECM plug seems to follow the same pattern, the border between expression domains was less defined.

TEM Analysis Shows Swollen ER, Autophagic Vacuoles, and Cell Death along with Disorganized ECM in the Healing Enthesis

The finding that the healing process of the enthesis involves local ECM secretion and cell loss formed the basis of studying this process at subcellular resolution. To this end, TEM was used to image both ends of the enthesis at 1 and 3 dpi. As seen in Figure 3A, at the tendon end of an uninjured control enthesis, typically elongated tenocytes with apparent nuclei and ER were observed. In contrast, 1 dpi, cells of injured entheses displayed an increased number of Golgi apparatus, swollen ER, and numerous vesicles with the morphology of autophagic vacuoles. At 3 dpi, the condition of these cells deteriorated, as lost nuclei, swollen ER, and damaged mitochondria were observed (Supplemental Figure S7A).

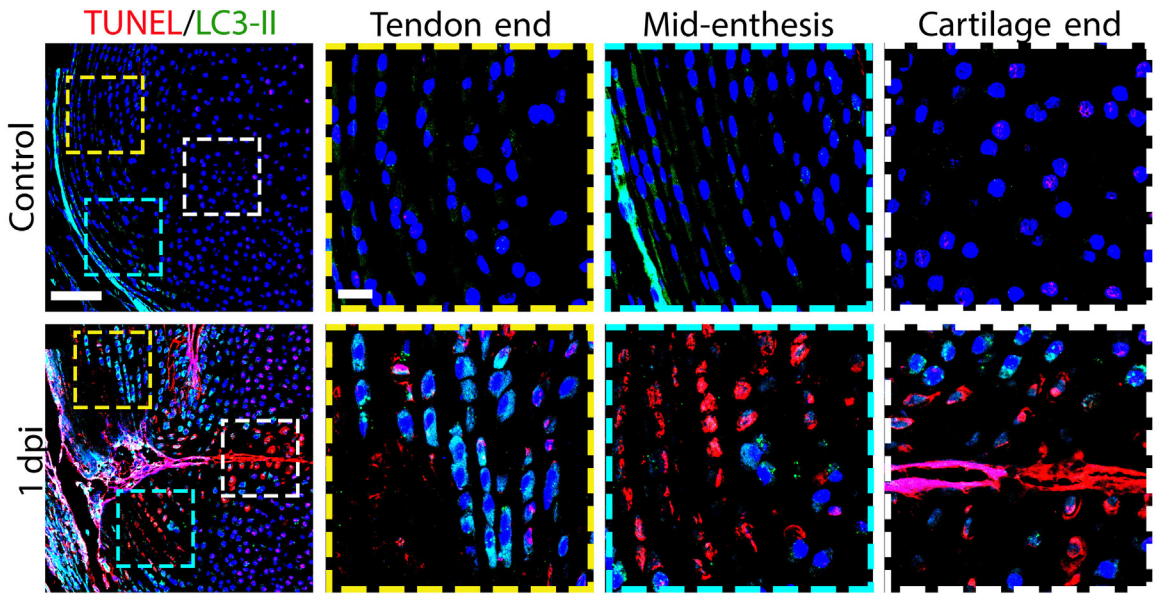

Figure 5 Molecular analyses for autophagy and cell death. Terminal deoxynucleotidyl transferase-mediated dUTP nick-end labeling (TUNEL) assay and immunohistochemical staining for autophagy marker LC3-II in control and 1-day after injury (dpi) mouse entheses. Magnifications of **boxed areas** show autophagic cells (marked in green) at the tendon end and near the injury site, along with apoptotic cells (marked in red), which were mainly located in mid-enthesis and cartilage end. Yellow, teal, and white boxes are magnifications of the **boxed areas.** $n = 5$. Scale bars: 100 μm (TUNEL/LC3-II images); 20 μm (**yellow, teal,** and **white boxed images**).

At the cartilage end of control enthesis, cells had a typical round shape of chondrocytes, with clear nuclei and extensive and well-organized ER (Figure 3B). However, adjacent to the injury site at 1 dpi, cells started to detach from the ECM around them and their membranes were ruptured, causing spillage of cell contents and membrane shedding. Internally, we observed less ER, nuclei became condensed, and mitochondria appeared damaged compared with control cells. As in the cells at the tendon end, autophagic vacuoles, swollen ER, and an increase in the number of Golgi apparatus were observed. However, the severity of these cellular pathologies was reduced relative to the opposite side. By 3 dpi, the condition of these cells dramatically deteriorated, as they lost their membranes as well as most of their organelles, including nuclei (Supplemental Figure S7B). The remains of the cell bodies were condensed in the center of their ECM lacunae. Interestingly, in the space that was left by the shrinking cells, ECM deposition was observed. This fit well with the finding of COL2A1 staining in the cell-free domains. Similarly, at 5 months after injury, the remains of the injured cells were still observed at both ends of the enthesis (Supplemental Figure S8).

The study next focused on the newly formed hypocellular domain and the ECM plug. At the tendon end of 1 dpi injured enthesis, unlike in the control, the collagen fibers were oriented in different directions (Figure 3C). At 3 dpi, collagen fibers remained disorganized, yet some alignment was observed. At the cartilage end, the ECM in the control enthesis was characterized by well-organized fibers. In contrast, in both 1 and 3 dpi injured entheses, the collagen

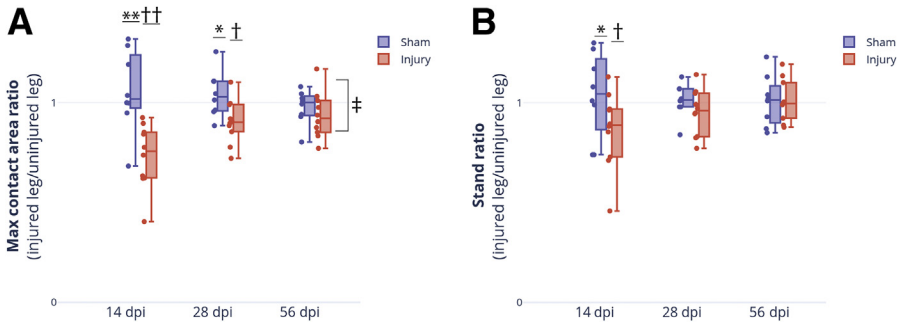

Figure 6 Enthesis healing restores its functional properties. Statistical analyses of CatWalk gait indices of maximum (Max) contact area ratio (**A**) and contact duration ratio (stand; **B**) of injured and sham-operated mice at 14, 28, and 56 days after manipulation. **Dashed line** denotes a ratio value of 1, indicating no difference in use of the manipulated leg relative to the contralateral leg. Data are presented as means ± SEM (**A** and **B**). $n = 10$ injured mice (**A** and **B**); $n = 8$ sham-operated mice (**A** and **B**). $^{*}P < 0.05$, $^{**}P < 0.01$, significant difference between injury and sham groups (independent-samples *t*-test); $^{\dagger}P < 0.05$, $^{\dagger\dagger}P < 0.01$, significantly different from a ratio value of 1 (independent-samples *t*-test); $^{\ddagger}P < 0.01$, main effect analysis showed that gait for injured limbs was significantly reduced in comparison to sham-operated limbs (two-factors analysis of variance). Dpi, days after injury.

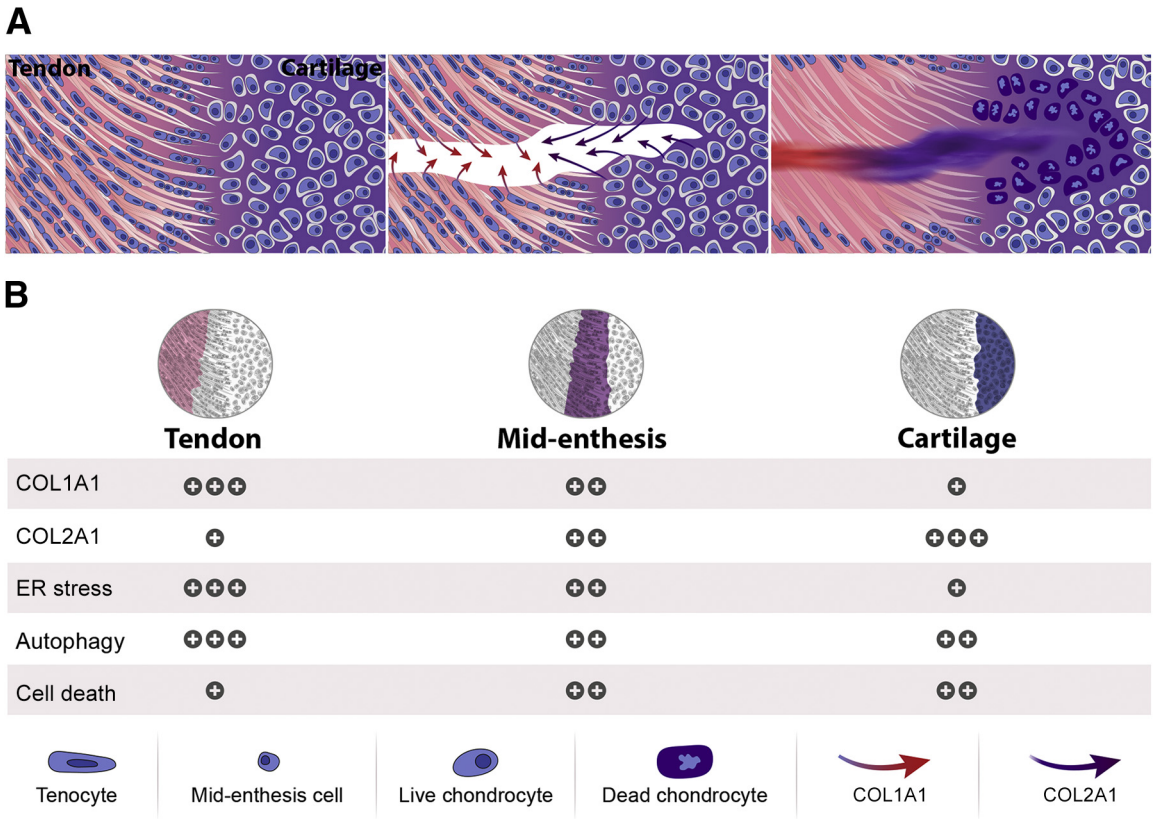

Figure 7 Variations in cellular response between the different regions of the injured neonatal enthesis during the formation of an acellular scar. **A: Left panel:** Illustrations of the neonatal enthesis before and after a needle-punch injury. **Middle panel:** Shortly after the injury, resident cells adjacent to the injury site secrete extracellular matrix (ECM) components corresponding to their cellular identity. **Right panel:** This process terminates in the formation of an acellular scar (healed enthesis). **Red arrows** mark collagen type I (COL1A1), and **purple arrows** mark collagen type II (COL2A1). **B:** Spatial distribution of ECM components and molecular markers following injury. Relative levels of expression are indicated by the number of plus signs (+, low; ++, medium; and +++, high). ER, endoplasmic reticulum.

fibers were misaligned, disorganized, and unevenly distributed.

Overall, the findings of increased Golgi apparatus, swollen ER, and autophagic vacuoles in the injured enthesis cells are consistent with extensive ECM production, which may also explain ECM disorganization as well as induction of ER stress and autophagy. The observation of shrinking cells that had lost their nuclei suggests that these cells underwent apoptotic cell death. Finally, these results indicate that the healing process involves different responses at the two ends of the enthesis.

The Injured Enthesis Undergoes ER Stress One Day after Injury

An increased secretory load during the formation of the ECM plug is expected to induce ER stress, as suggested by our finding of swollen ER in cells near the injury site. To address this possibility, we measured the expression of ER stress markers *BiP* and *CHOP*. For that, mRNA was isolated from all regions of 1 dpi Achilles entheses (tendon, mid enthesis, and cartilage) and from uninjured control entheses. Quantitative real-time PCR revealed a significant elevation of both markers in the injured tissues compared with the control, suggesting that cells at the injured enthesis undergo ER stress (Figure 4A). To verify this result and to localize the cells that undergo ER stress, single-molecule fluorescence *in situ* hybridization was performed for both markers on sections of 1 dpi and control entheses (Figure 4B). Quantification showed that both markers were significantly elevated at the tendon end of the mid-enthesis, whereas at the cartilage end, only *BiP* was significantly increased (Figure 4C). These results confirmed the induction of ER stress in the enthesis during the healing process as indicated by quantitative real-time PCR, supporting the notion that enthesis cells were under a heavy burden of ECM secretion. Furthermore, they indicate a difference in the healing responses between the two sides of the enthesis.

Enthesis Healing Involves Autophagy and Cell Death

TEM analysis identified cellular features consistent with autophagy and cell death in the injured tissue. To confirm the occurrence of these processes, molecular markers involved in these processes were tracked. To examine the expression of the autophagy marker LC3-II, the study

applied our injury procedure to GFP-LC3 mice[43] and analyzed their entheses at 1 dpi. As seen in Figure 5, many LC3-II–positive cells were observed at the tendon end, whereas few LC3-II–positive cells were observed in the middle of the enthesis and cartilage. These results support the TEM observation and suggest that the healing process involves autophagy, most prominently at the tendon end of the injured tissue.

Previous studies of injured articular cartilage describe a cell death process known as chondroptosis. This variant of apoptosis is characterized by an increase in the amount of Golgi apparatus and ER, autophagic vacuoles, patchy condensations of nuclei, blebbing of cytoplasmic material,[16] TUNEL-positive cells,[44] and activation of caspase-3 and caspase-9.[45] Because our TEM analysis revealed several of these features, the injury site for cell death was examined by applying TUNEL assay to sections of 1 dpi entheses. At the tendon end, a few cells were TUNEL positive; however, the signal was dramatically increased in mid-enthesis and on the cartilage end. Next, immunostaining was performed for cleaved (ie, activated) caspase-3 (Supplemental Figure S9); however, no signal was detected in or around the injury site. Cellular morphology suggested that the death mechanism was similar to chondroptosis; however, the lack of caspase-3 cleavage suggests that these cells activate a different cell death program.

Together, these results suggest that the different compartments of the injured enthesis undergo both autophagy and cell death.

Healing of Neonatal Enthesis via Formation of Hypocellular Domains Flanking an ECM Plug Restores the Functional Properties of the Joint

To determine whether enthesis healing resulted in restoration of limb function, the gait and stride was examined in needle-punched and sham-operated animals at 14, 28, and 56 dpi using the CatWalk system. As depicted in Figure 6A, at 14 dpi, the maximum contact area ratio between injury side and contralateral paws was significantly reduced compared with sham mice, indicating that the mice avoided using the paw of the injured leg. This difference was reduced at 28 dpi, and by 56 dpi, both injured and sham mice displayed similarly high ratios, indicating restoration of leg function and gait. A similar pattern was found for the ratio between print areas (Supplemental Figure S10), whereas for contact duration ratio (stand), a significant difference at 14 dpi was reduced already by 28 dpi (Figure 6B). Together, these results suggest that 56 days after the injury, the enthesis regained its function.

Discussion

In this work, partial injuries were induced to Achilles entheses of neonatal mice to uncover the ensuing healing sequence in the different regions of this complex tissue. Restoration of enthesis function was correlated with an extensive local secretion of ECM, which formed a plug that sealed the lesion, concomitant with cell loss that resulted in an acellular scar tissue flanking the lesion (Figure 7A). Interestingly, the cellular response to the injury varied along the enthesis. At the tendon end, most cells underwent ER stress and autophagy; however, few cells in the cartilage end underwent these processes. Conversely, cell death was more prominent at the cartilage end (Figure 7B). These results suggest a differential cellular response along the healing enthesis.

In adult tissues, wound healing typically involves infiltration of phagocytes and fibroblasts into the injury site, where they secrete proinflammatory cytokines, chemokines, and growth factors to promote phagocytosis, angiogenesis, cell proliferation, and deposition of collagen, predominantly COL3A1.[46] Usually, this process terminates by formation of a hypercellular fibrovascular scar.[1,2,47,48] The current findings in the injured neonatal enthesis deviate from the common model in several ways. First, there was no recruitment of blood vessels, immune cells, or fibroblasts to the injury site. Second, the composition of the scar tissue differed from the typical adult fibrovascular scar, as it was hypocellular and its ECM content changed from COL2A1 at the cartilage side to COL1A1 at the tendon side. In the transition area, a mixture of both collagen types was found. Third, the secretory cells that formed the scar tissue were resident cells of the enthesis. Fourth, the process involved ER stress, autophagy, and cell death of the resident secretory cells.

The identity of signals that induce the healing process and the extensive ECM secretion is still an open question. These signals may be molecular, mechanical, or a combination of the two. Putative molecular signals that may drive the process were previously observed in vertebrate and in *Drosophila*.[49–52] In both cases, the apoptotic cells produced a signal that propagated away and could induce either survival or apoptosis in neighboring cells. However, the enthesis is also a mechanosensitive tissue and, therefore, healing may have also been affected by biophysical forces.[26,53,54] Moreover, developmental studies have shown that mechanical load is essential for the formation of a proper enthesis.[55–57] It is possible that because of the injury, the loss of tissue integrity alternates the mechanical signals that the enthesis cells receive, leading to their activation. Another interesting characteristic of the healing process observed in the current study is the propagation of the injury signal several rows of cells away from the margins of the injury site, causing the death of cells that were not directly damaged by the penetrating needle. Whether this propagation was mediated by the original signals that initiated the healing process, or by another mechanism, requires further investigation.

The study showed that during the healing process, resident cells activated ER stress, autophagy, and cell death

programs in a region-specific manner. ER stress is commonly associated with extensive ECM production, as the protein load on the ER exceeds its folding capacity.[58] Although this stress response is a coping mechanism, prolonged ER stress can disturb cellular homeostasis and cause cell death.[59,60] In addition, in response to ER stress, autophagy may be triggered to restore homeostasis and to provide an alternative source of intracellular building blocks and energy to the cell.[58] Although in some cases, autophagy following ER stress has a prosurvival effect, in other cases, it promotes self-consumption and cell death.[61–63] Programmed cell death pathways, which are identified by morphologic and molecular markers, can be triggered by different stimuli.[64] In the current study, although the dying cells in the cartilage end displayed features of chondroptosis, other characteristics were missing. Therefore, the cell death pathway that we observed may be novel. Different responses were seen on the tendon end compared with the cartilage end of the healing enthesis. The epistatic relations between these cellular phenotypes and their role in the healing process are unknown. Nevertheless, their variable distribution suggests that among the cell types of the enthesis, there are different strategies of coping with the injury and with the consequent high demand for collagen production.

Previous studies have shown that in the adult enthesis, the healing process is characterized by the formation of a hypercellular and vascularized scar.[27,65,66] It is plausible that many of the differences between our observations and previous ones could be driven by age differences. Yet, other factors might contribute to the different outcomes as well. The study used a needle punch to injure the enthesis and took great care not to reach the marrow space. In contrast, previous studies have included partial or full detachment of the tendon, reattachment of the tendon to bone, or punch defects that entered the marrow space.[67] Furthermore, injury to deeper structures, such as the supraspinatus tendon enthesis, requires dissection of surrounding muscles, which can trigger bleeding and infiltration of cells and factors derived from the vasculature.[28] These extrinsic factors may complicate the interpretation of healing mechanisms. In the current neonatal Achilles enthesis injury model, no signs of inflammation were seen at the injury site, a result likely resulting from the s.c. position of the enthesis, which lacks overlying musculature, and the poor vascularization.[26,53] These local conditions may limit the ability of chemotaxis and infiltration of immune cells and fibroblasts into the injury site. The effect of local conditions on the healing process was previously observed in a comparison between two different anatomic locations of canine flexor tendon (namely, the poorly vascularized intrasynovial part and the well-vascularized extrasynovial part). Although injury to the extrasynovial part led to angiogenesis, inflammation, and repair, the healing intrasynovial part showed minimal vascularization and muted inflammation, resulting in poor repair.[8]

Finally, although mechanical testing of the healed enthesis was not performed, gait analysis indicated that the function of the injured leg improved considerably by 2 months after injury. This suggests that despite the unusual nature of the healing process and the resulting acellular scar, the newly produced tissue is functional. Nonetheless, injury was induced before the postnatal mineralization of the maturing enthesis, which could have contributed to functional restoration.

In conclusion, the current findings provide insight into the healing of the injured neonatal enthesis and present a novel healing mechanism. The key feature of this healing process is the formation of a hypocellular scar by resident cells. The finding of different cellular responses along the length of the enthesis reveals a new level of complexity of this transitional tissue. Recently, the neonatal mouse has emerged as a model for improved healing capacities in diverse mammalian tissues compared with adults, in which injury often fails to heal or terminates with a fibrotic scar.[10,29,68–70] Identifying the mechanisms that regulate this new healing process may therefore lead to the development of new approaches to the treatment of adult tendon enthesis injuries.

Acknowledgments

We thank Nitzan Konstantin for expert editorial assistance; Prof. Zvulun Elazar (Weizmann Institute of Science) for kindly providing green fluorescent protein–LC3#53 mice; Dr. Ron Rotkopf (Weizmann Institute of Science) for help with statistical analyses; Tali Wiesel and Tal Bigdary (Weizmann Institute of Science) for help with graphics; Aaron Vinestock for assistance with single-molecule fluorescence *in situ* hybridization quantification; and all members of the Zelzer laboratory for encouragement and advice.

Author Contributions

R.C.V. conceptualized the study, devised methodology, investigated, formally analyzed, and visualized the results, and wrote original draft; N.F. conceptualized the study, devised methodology, and investigated the study; E.A., E.K., and S.K. investigated the study; S.R. devised methodology; L.H.-Y. formally analyzed the study; N.D. and S.L.-Z. investigated the study; M.T. investigated the study and formally analyzed the results; S.T. conceptualized the study and wrote original draft; and E.Z. conceptualized the study, devised methodology, supervised, and wrote original draft.

Supplemental Data

Supplemental material for this article can be found at *http://doi.org/10.1016/j.ajpath.2022.05.008*.

References

1. Darby IA, Desmoulière A: Scar formation: cellular mechanisms. Textbook on Scar Management. Edited by Téot L, Mustoe TA, Middelkoop E, Gauglitz GG. Cham, Switzerland: Springer International Publishing, 2020. pp. 19–26
2. Stroncek JD, Reichert WM: Overview of wound healing in different tissue types. Indwelling Neural Implants: Strategies for Contending with the In Vivo Environment. Boca Raton, FL: CRC Press, 2007. pp. 3–38
3. Shen W, Ferretti M, Manley M, Fu F: Musculoskeletal fundamentals: form, function, and a survey of healing strategies. Musculoskeletal Tissue Regeneration: Biological Materials and Methods. Totowa, NJ: Humana Press, 2008. pp. 19–38
4. Dimitriou R, Jones E, McGonagle D, Giannoudis PV: Bone regeneration: current concepts and future directions. BMC Med 2011, 9:66
5. Chargé SBP, Rudnicki MA: Cellular and molecular regulation of muscle regeneration. Physiol Rev 2004, 84:209–238
6. Hunziker EB: Articular cartilage repair: basic science and clinical progress: a review of the current status and prospects. Osteoarthr Cartil 2002, 10:432–463
7. Frank CB, Hart DA, Shrive NG: Molecular biology and biomechanics of normal and healing ligaments - a review. Osteoarthr Cartil 1999, 7: 130–140
8. Shen H, Yoneda S, Sakiyama-elbert SE, Zhang Q, Thomopoulos S: Flexor tendon injury and repair: the influence of synovial environment on the early healing response in a canine model. J Bone Joint Surg Am 2021, 103:e50
9. Thomopoulos S, Parks WC, Rifkin DB, Derwin KA: Mechanisms of tendon injury and repair. J Orthop Res 2015, 33:832–839
10. Howell K, Chien C, Bell R, Laudier D, Tufa SF, Keene DR, Andarawis-Puri N, Huang AH: Novel model of tendon regeneration reveals distinct cell mechanisms underlying regenerative and fibrotic tendon healing. Sci Rep 2017, 7:1–14
11. Dyment NA, Hagiwara Y, Matthews BG, Li Y, Kalajzic I, Rowe DW: Lineage tracing of resident tendon progenitor cells during growth and natural healing. PLoS One 2014, 9:1–12
12. Voleti PB, Buckley MR, Soslowsky LJ: Tendon healing: repair and regeneration. Annu Rev Biomed Eng 2012, 14:47–71
13. Docheva D, Müller SA, Majewski M, Evans CH: Biologics of tendon repair. Adv Drug Deliv Rev 2015, 84:222–239
14. Lin D, Alberton P, Caceres MD, Volkmer E, Schieker M, Docheva D: Tenomodulin is essential for prevention of adipocyte accumulation & fibrovascular scar formation during early tendon healing. Cell Death Dis 2017, 8:e3116
15. Redman SN, Oldfield SF, Archer CW, Roughley PJ, Lee C: Current strategies for articular cartilage repair. Eur Cells Mater 2005, 9: 23–32
16. Roach HI, Aigner T, Kouri JB: Chondroptosis: a variant of apoptotic cell death in chondrocytes? Apoptosis 2004, 9:265–277
17. Battistelli M, Salucci S, Olivotto E, Facchini A, Minguzzi M, Guidotti S, Pagani S, Flamigni F, Borzì RM, Facchini A, Falcieri E: Cell death in human articular chondrocyte: a morpho-functional study in micromass model. Apoptosis 2014, 19:1471–1483
18. Sitte I, Klosterhuber M, Lindtner RA, Freund MC, Neururer SB, Pfaller K, Kathrein A: Morphological changes in the human cervical intervertebral disc post trauma: response to fracture-type and degeneration grade over time. Eur Spine J 2016, 25:80–95
19. Almonte-Becerril M, Navarro-Garcia F, Gonzalez-Robles A, Vega-Lopez MA, Lavalle C, Kouri JB: Cell death of chondrocytes is a combination between apoptosis and autophagy during the pathogenesis of osteoarthritis within an experimental model. Apoptosis 2010, 15:631–638
20. Sitte I, Kathrein A, Pfaller K, Pedross F, Roberts S: Intervertebral disc cell death in the porcine and human injured cervical spine after trauma: a histological and ultrastructural study. Spine (Phila Pa 1976) 2009, 34:131–140
21. Jiang LB, Liu HX, Zhou YL, Sheng SR, Xu HZ, Xue EX: An ultrastructural study of chondroptosis: programmed cell death in degenerative intervertebral discs in vivo. J Anat 2017, 231:129–139
22. Matsiko A, Levingstone TJ, O'Brien FJ: Advanced strategies for articular cartilage defect repair. Materials (Basel) 2013, 6:637–668
23. Hunziker EB: Articular cartilage repair: are the intrinsic biological constraints undermining this process insuperable? Osteoarthr Cartil 1999, 7:15–28
24. Newman AP: Articular cartilage repair. Am J Sports Med 1998, 26: 309–324
25. Doschak MR, Zernicke RF: Structure, function and adaptation of bone-tendon and bone-ligament complexes. J Musculoskelet Neuronal Interact 2005, 5:35–40
26. Zelzer E, Blitz E, Killian ML, Thomopoulos S: Tendon-to-bone attachment: from development to maturity. Birth Defects Res C Embryo Today 2014, 102:101–112
27. Derwin KA, Galatz LM, Ratcliffe A, Thomopoulos S: Enthesis repair: challenges and opportunities for effective tendon-to-bone healing. J Bone Joint Surg Am 2018, 100:e109
28. Moser HL, Doe AP, Meier K, Garnier S, Laudier D, Akiyama H, Zumstein MA, Galatz LM, Huang AH: Genetic lineage tracing of targeted cell populations during enthesis healing. J Orthop Res 2018, 36:3275–3284
29. Schwartz AG, Galatz LM, Thomopoulos S: Enthesis regeneration: a role for Gli1+ progenitor cells. Development 2017, 144:1159–1164
30. Kawamoto T, Kawamoto K: Preparation of thin frozen sections from nonfixed and undecalcified hard tissues using Kawamot's film method (2012). Methods Mol Biol 2014, 1130:149–164
31. Bemenderfer TB, Harris JS, Condon KW, Li J, Kacena MA: Processing and sectioning undecalcified murine bone specimens. Methods Mol Biol 2021, 2230:231–257
32. Choi HMT, Schwarzkopf M, Fornace ME, Acharya A, Artavanis G, Stegmaier J, Cunha A, Pierce NA: Third-generation in situ hybridization chain reaction: multiplexed, quantitative, sensitive, versatile, robust. Development 2018, 145:1–10
33. Shwartz Y, Zelzer E: Nonradioactive in situ hybridization on skeletal tissue sections. Skeletal Development and Repair: Methods in Molecular Biology. Edited by Hilton MJ. Totowa, NJ: Humana Press, 2014. pp. 203–215
34. Schindelin J, Arganda-Carreras I, Frise E, Kaynig V, Longair M, Pietzsch T, et al: Fiji: an open-source platform for biological-image analysis. Nature Methods 2012, 9:676–682
35. Stirling DR, Swain-Bowden MJ, Lucas AM, Carpenter AE, Cimini BA, Goodman A: CellProfiler 4: improvements in speed, utility and usability. BMC Bioinformatics 2021, 22:433
36. Deumens R, Jaken RJP, Marcus MAE, Joosten EAJ: The CatWalk gait analysis in assessment of both dynamic and static gait changes after adult rat sciatic nerve resection. J Neurosci Methods 2007, 164: 120–130
37. Kappos EA, Sieber PK, Engels PE, Mariolo AV, D'Arpa S, Schaefer DJ, Kalbermatten DF: Validity and reliability of the CatWalk system as a static and dynamic gait analysis tool for the assessment of functional nerve recovery in small animal models. Brain Behav 2017, 7:e00723
38. Perry RB-T, Doron-Mandel E, Iavnilovitch E, Rishal I, Dagan SY, Tsoory M, Coppola G, McDonald MK, Gomes C, Geschwind DH, Twiss JL, Yaron A, Fainzilber M: Subcellular knockout of importin β1 perturbs axonal retrograde signaling. Neuron 2012, 75:294–305
39. Austyn JM, Gordon S: F4/80, a monoclonal antibody directed specifically against the mouse macrophage. Eur J Immunol 1981, 11: 805–815
40. DeLisser HM, Newman PJ, Albelda SM: Molecular and functional aspects of PECAM-1/CD31. Immunol Today 1994, 15:490–495
41. Thomopoulos S, Hattersley G, Rosen V, Mertens M, Galatz L, Williams GR, Soslowsky LJ: The localized expression of extracellular matrix components in healing tendon insertion sites: an in situ hybridization study. J Orthop Res 2002, 20:454–463

42. Zhang J, Yuan T, Zheng N, Zhou Y, Hogan MV, Wang JHC: The combined use of kartogenin and platelet-rich plasma promotes fibrocartilage formation in the wounded rat Achilles tendon entheses. Bone Joint Res 2017, 6:231−244
43. Mizushima N: Methods for monitoring autophagy using GFP-LC3 transgenic mice. Methods in Enzymology. ed 1. London, UK: Elsevier Inc, 2009
44. Pérez HE, Luna MJ, Rojas ML, Kouri JB: Chondroptosis: an immunohistochemical study of apoptosis and Golgi complex in chondrocytes from human osteoarthritic cartilage. Apoptosis 2005, 10:1105−1110
45. Hwang HS, Kim HA: Chondrocyte apoptosis in the pathogenesis of osteoarthritis. Int J Mol Sci 2015, 16:26035−26054
46. Goldberg SR, Diegelmann RF: Basic science of wound healing. Critical Limb Ischemia. Edited by Dieter RS, Dieter RA Jr, Dieter RA III, Nanjundappa A. Cham, Switzerland: Springer International Publishing, 2017. pp. 131−136
47. Li J, Chen J, Kirsner R: Pathophysiology of acute wound healing. Clin Dermatol 2007, 25:9−18
48. Chen GY, Nuñez G: Sterile inflammation: sensing and reacting to damage. Nat Rev Immunol 2010, 10:826−837
49. Pérez-Garijo A, Fuchs Y, Steller H: Apoptotic cells can induce non-autonomous apoptosis through the TNF pathway. Elife 2013, 2: e01004
50. Amcheslavsky A, Lindblad JL, Bergmann A: Transiently "undead" enterocytes mediate homeostatic tissue turnover in the adult drosophila midgut. Cell Rep 2020, 33:108408
51. Valon L, Davidović A, Levillayer F, Villars A, Chouly M, Cerqueira-Campos F, Levayer R: Robustness of epithelial sealing is an emerging property of local ERK feedback driven by cell elimination. Dev Cell 2021, 56:1700−1711.e8
52. Gagliardi PA, Dobrzyński M, Jacques MA, Dessauges C, Ender P, Blum Y, Hughes RM, Cohen AR, Pertz O: Collective ERK/Akt activity waves orchestrate epithelial homeostasis by driving apoptosis-induced survival. Dev Cell 2021, 56:1712−1726.e6
53. Benjamin M, Toumi H, Ralphs JR, Bydder G, Best TM, Milz S: Where tendons and ligaments meet bone: attachment sites ('entheses') in relation to exercise and/or mechanical load. J Anat 2006, 208: 471−490
54. Thomopoulos S, Genin GM, Galatz LM: The development and morphogenesis of the tendon-to-bone insertion - what development can teach us about healing. J Musculoskelet Neuronal Interact 2010, 10:35−45
55. Butler RJ, Marchesi S, Royer T, Davis IS: The effect of a subject-specific amount of lateral wedge on knee. J Orthop Res 2007, 25: 1121−1127
56. Schwartz AG, Lipner JH, Pasteris JD, Genin GM, Thomopoulos S: Muscle loading is necessary for the formation of a functional tendon enthesis. Bone 2013, 55:44−51
57. Blitz E, Viukov S, Sharir A, Shwartz Y, Galloway JL, Pryce BA, Johnson RL, Tabin CJ, Schweitzer R, Zelzer E: Bone ridge patterning during musculoskeletal assembly is mediated through SCX regulation of Bmp4 at the tendon-skeleton junction. Dev Cell 2009, 17:861−873
58. Høyer-Hansen M, Jäättelä M: Connecting endoplasmic reticulum stress to autophagy by unfolded protein response and calcium. Cell Death Differ 2007, 14:1576−1582
59. Rao RV, Ellerby HM, Bredesen DE: Coupling endoplasmic reticulum stress to the cell death program. Cell Death Differ 2004, 11:372−380
60. Lin JH, Walter P, Yen TSB: Endoplasmic reticulum stress in disease pathogenesis. Annu Rev Pathol Mech Dis 2008, 3:399−425
61. Song S, Tan J, Miao Y, Li M, Zhang Q: Crosstalk of autophagy and apoptosis: involvement of the dual role of autophagy under ER stress. J Cell Physiol 2017, 232:2977−2984
62. Rashid HO, Yadav RK, Kim HR, Chae HJ: ER stress: autophagy induction, inhibition and selection. Autophagy 2015, 11:1956−1977
63. Hetz C, Papa FR: The unfolded protein response and cell fate control. Mol Cell 2018, 69:169−181
64. Galluzzi L, Vitale I, Aaronson SA, Abrams JM, Adam D, Agostinis P, et al: Molecular mechanisms of cell death: recommendations of the Nomenclature Committee on Cell Death 2018. Cell Death Differ 2018, 25:486−541
65. Smietana MJ, Moncada-Larrotiz P, Arruda EM, Bedi A, Larkin LM: Tissue-engineered tendon for enthesis regeneration in a rat rotator cuff model. Biores Open Access 2017, 6:47−57
66. Apostolakos J, Durant TJS, Dwyer CR, Russell RP, Weinreb JH, Alaee F, Beitzel K, McCarthy MB, Cote MP, Mazzocca AD: The enthesis: a review of the tendon-to-bone insertion. Muscles Ligaments Tendons J 2014, 4:333−342
67. Moser HL, Abraham AC, Howell K, Laudier D, Zumstein MA, Galatz LM, Huang AH: Cell lineage tracing and functional assessment of supraspinatus tendon healing in an acute repair murine model. J Orthop Res 2021, 39:1789−1799
68. Porrello ER, Mahmoud AI, Simpson E, Hill JA, Richardson JA, Olson EN, Sadek HA: Transient regenerative potential of the neonatal mouse heart. Science 2011, 331:1078−1080
69. Han M, Yang X, Lee J, Allan CH, Muneoka K: Development and regeneration of the neonatal digit tip in mice. Dev Biol 2008, 315: 125−135
70. Torre OM, Das R, Berenblum RE, Huang AH, Iatridis JC: Neonatal mouse intervertebral discs heal with restored function following herniation injury. FASEB J 2018, 32:4753−4762